Water-soluble rhenium clusters with triazoles: the effect of chemical structure on cellular internalization and the DNA binding of the complexes

Dmitry I. Konovalov,[a] Anton A. Ivanov,[a] Tatiana S. Frolova,[b,c] Ilia V. Eltsov,[b] Yakov M. Gayfulin,[a] Louis Plunkett,[d] Masoomeh Bazzar,[d] Ali M. Adawi,[d] Jean-Sebastien G. Bouillard,[d] Sergey I. Baiborodin,[c] Olga I. Sinitsyna,[b,c] Natalia V. Kuratieva,[a] Vadim V. Yanshole,[a,b,e] Olga A. Efremova,*[d] Michael A. Shestopalov*[a]

[a]   D.I. Konovalov, Dr. A.A. Ivanov, Dr. Y.M. Gayfulin, Dr. N.V. Kuratieva, Dr. V.V. Yanshole, Dr. M.A. Shestopalov
       Nikolaev Institute of Inorganic Chemistry SB RAS
       3 acad. Lavrentiev ave., 630090 Novosibirsk (Russia)
       E-mail: shtopy@niic.nsc.ru (M.A. Shestopalov)
[b]   Dr. T.S. Frolova, Dr. I.V. Eltsov, Dr. O.I. Sinitsyna, Dr. V.V. Yanshole
       Novosibirsk State University
       2 Pirogova st., 630090 Novosibirsk (Russia)
[c]   Dr. T.S. Frolova, Dr. S.I. Baiborodin, Dr. O.I. Sinitsyna
       Federal Research Center Institute of Cytology and Genetics SB RAS
       10 acad. Lavrentiev ave., 630090 Novosibirsk (Russia)
[d]   L. Plunkett, M. Bazzar, Dr. A.M. Adawi, Dr. J.-S.G. Bouillard, Dr. O.A. Efremova
       School of Mathematics and Physical Sciences
       G.W. Gray Centre for Advanced Materials University of Hull
       Cottingham Road, HU6 7RX, Hull (UK)
       E-mail : olgaa.efremova@gmail.com (O.A. Efremova)
[e]   Dr. V.V. Yanshole
       International Tomography Centre SB RAS
       3a Institutskaya st., 630090 Novosibirsk (Russia)

       Supporting information for this article is given via a link at the end of the document.

Abstract: Here we explore the effect of the nature of organic ligands in rhenium cluster complexes $[Re_6Q_8L_6]^{4-}$ (where Q=S or Se, and L=benzotriazole, 1,2,3-triazole or 1,2,4-triazole) on the biological properties of the complexes, in particular on the cellular toxicity, cellular internalization and localization. Specifically, the paper describes the synthesis and detailed characterization of the structure, luminescence and electrochemical properties of the four new Re_6 clusters with 1,2,3- and 1,2,4-triazoles. Biological assays of these complexes are also discussed in addition to those with benzotriazole using cervical cancer (HeLa) and immortalized human fibroblasts (CRL-4025) as model cell lines. Our study demonstrates that the presence of hydrophobic and π-bonding rich units such as the benzene ring in benzotriazole significantly enhances cellular internalization of rhenium clusters. These ligands facilitate binding of the clusters to DNA, which results in increased cytotoxicity of the complexes.

Introduction

Octahedral rhenium cluster complexes with the general formula $[\{Re_6Q_8\}L_6]^n$ (Q = S, Se, Te) have gathered significant interest due to their good phosphorescence properties in red/near infrared region of the spectrum,[1] high X-ray attenuation,[2] and their ability to generate singlet oxygen.[3] Hence these cluster have a high potential for applications associated with photodynamic inactivation of malignant cells and bacteria. Moreover, octahedral rhenium clusters have significantly higher chemical, electrochemical and thermal stability than their molybdenum and tungsten analogues.

Despite having such superb properties, only a handful of complexes were tested in biomedical (bioimaging and biolabeling,[4] as X-ray contrast agents[2] or photodynamic therapy (PDT)[3b]) and materials-based applications (e.g. organic light-emitting diodes (OLEDs)[5] and liquid crystals[6]). In the context of the biological applications, there is an obstacle associated with the limited choice of water-soluble octahedral rhenium clusters. Indeed, up until recently the known water-soluble clusters were those with the inorganic, highly hydrophilic ligands, CN^- and OH^-.[7] Although these complexes demonstrated high biomedical potential, the scarcity of such hydrophilic ligands cannot offer much freedom to fine-tune biologically active properties, in particular cellular internalization profiles and cellular localization of the complexes to suit particular biomedical applications. For example, optical bioimaging and PDT agents must in some way participate in intracellular processes or interact with components participating in the processes. Therefore, such diagnostics and therapies require agents with good cellular internalization and preferably targeted localization within the cells (e.g. in the perinuclear region in case of PDT), while X-ray contrast agents should display the least possible interaction with body constituents and processes to offer greater patient tolerance.[8]

To expand our understanding of the biological potential of octahedral rhenium complexes and to be able to tune their biological properties, our group has developed new methods to synthesize octahedral rhenium clusters that bear organic ligands.[4b, 9] Namely, octahedral rhenium cluster complexes with organic ligands can be obtained by the direct reaction of fully inorganic cluster precursors in molten organic pro-ligand at relatively high temperature (150-200 °C) or using a solvothermal process. For example, using these approaches the first water-

soluble rhenium cluster complexes with organic phosphine-based ligands $Na_4[\{Re_6Q_8\}(PPh_2CH_2CH_2COO)_6]$ (Q = S, Se),[9b] $Na_2\{H\}_{14}[\{Re_6Q_8\}(P(CH_2CH_2COO)_3)_6]$ (Q = S, Se)[9d] and $Na_2\{H\}_8[\{Re_6Se_8\}(P(CH_2CH_2CONH_2)(CH_2CH_2COO)_2)_6]$ were obtained.[9c, 10] The cellular internalization of these complexes was studied on larynx carcinoma (Hep-2) and cervical cancer (HeLa) cell lines. The studies indeed demonstrated that compounds with a dual-nature (hydrophilic and hydrophobic) ligand $PPh_2CH_2CH_2COOH$ are readily taken in by the cells with localization in cytoplasm, while highly negatively charged complexes with hydrophilic ligands $(P(CH_2CH_2COO)_3)^{3-}$ or $(P(CH_2CH_2CONH_2)(CH_2CH_2COO)_2)^{2-}$ were not taken in by the cells. On the other hand, cytotoxicity and acute *in vivo* toxicity patterns of the complexes was influenced not only by the ability of the complex to internalize into the cells but also by the number of ions a complex produces in a solution. Indeed, it was demonstrated by *in vitro* and *in vivo* studies that the toxicity of $Na_2\{H\}_8[\{Re_6Se_8\}(P(C_2H_4CONH_2)(C_2H_4COO)_2)_6]$ aqueous solutions was considerably lower than $Na_2\{H\}_{14}[\{Re_6Q_8\}(P(CH_2CH_2COO)_3)_6]$ with a fully hydrolyzed ligand in the form of $P(C_2H_4COOH)_3$ due to higher osmolality of the latter.[9d]

Reactions of $K_4[Re_6Q_8(OH)_6]$ (Q = S, Se) in molten benzotriazole (btrzH) pro-ligand also lead to water-soluble compounds $[\{Re_6Q_8\}(btrz)_6]^{4-}$ (Q = S, Se).[4b] Studies on Hep-2 cells demonstrated that the complexes internalized well into the cells with predominant localization in perinuclear area. These complexes were shown to be at least 10-fold more cytotoxic than the equivalent phosphine analogues.

In this work, we were keen to explore the effect of the benzene ring within benzotriazole on their cellular toxicity, internalization and localization of the rhenium cluster complexes in more detail. To do that we have synthesized and characterized new rhenium cluster complexes $[\{Re_6Q_8\}(L)_6]^{4-}$, where Q = S and L = 1,2,3-triazolate (1,2,3-trz) (**1**), Q = Se and L = 1,2,3-triazolate (**2**), Q = S and L = 1,2,4-triazolate (1,2,4-trz) (**3**), or Q = Se and L = 1,2,4-triazolate (**4**) to compare their biological properties, such as cytotoxicity and genotoxicity, internalization and localization within the HeLa and CRL-4025 (immortalized human fibroblasts) to those of $[\{Re_6Q_8\}(btrz)_6]^{4-}$ (Q = S (**5**), Se (**6**)) (Table 1).

Table 1. Abbreviations of compounds used in the manuscript.

Compound	Abbreviation
$[\{Re_6S_8\}(1,2,3\text{-}trz)_6]^{4-}$	**1**
$[\{Re_6Se_8\}(1,2,3\text{-}trz)_6]^{4-}$	**2**
$[\{Re_6S_8\}(1,2,4\text{-}trz)_6]^{4-}$	**3**
$[\{Re_6Se_8\}(1,2,4\text{-}trz)_6]^{4-}$	**4**
$[\{Re_6S_8\}(btrz)_6]^{4-}$	**5**
$[\{Re_6Se_8\}(btrz)_6]^{4-}$	**6**

The synthesis and characterization of rhenium complexes with benzotriazole, $K_4[\{Re_6S_8\}(btrz)_6]\cdot3.5EtOH\cdot4H_2O$ (K_4-**5**·3.5EtOH·4H₂O) and $K_{2.75}H_{1.25}[\{Re_6Se_8\}(btrz)_6]\cdot3EtOH\cdot7H_2O$ (K_4-**6**·3EtOH·7H₂O) has been reported before.[4b] In order to eliminate the toxic effects of K^+ ions and to increase the solubility of the compounds, sodium salts of the cluster complexes were used for biological studies. Sodium salts $Na_4[\{Re_6Q_8\}(btrz)_6]$ (Na_4-**5** and Na_4-**6**) were obtained in a similar fashion, *i.e.* the reaction of sodium salt of hydroxo clusters $[\{Re_6Q_8\}(OH)_6]^{4-}$ (Q = S or Se) using corresponding molten pro-ligands as reaction media. Indeed, our previous systematic studies demonstrated that such reactions, where a reactive pro-ligand is a protic agent, lead to a complete substitution of all six apical ligands.[4b, 9b, 11] The reaction melts were dissolved in ethanol and crystallized as neat Na_4-**5** and Na_4-**6**. Elemental analyses, NMR (Fig. S1-S6), EDX and FTIR unambiguously confirmed the similarity of the sodium cluster complex to the potassium analogue.

Although the overall approach for the synthesis of octahedral clusters bearing 1,2,3-triazole and 1,2,4-triazole is generally the same, the isolation of the neat complexes was more complicated. Unlike benzotriazole complexes, precipitation of anions **1-4** from the ethanol solutions of the melts resulted in solvates $Cat_4[\{Re_6Q_8\}L_6]\cdot x(LH)\cdot y(H_2O)\cdot z(EtOH)$, *i.e.* co-precipitated with molecules of the triazoles. The isolation of the neat complexes required a few extra steps: the conversion of the salt into the neutral water-insoluble $[\{Re_6Q_8\}(LH)_4L_2]$ with the help of 1M HCl, a few washing cycles with water followed by the conversion of the neutral complex back into the salt and finally recrystallization from DMSO by precipitation of the neat product with ethyl acetate. The product, as assessed by CHNS analysis, sometimes contained 1-2 molecules of DMSO per formula unit, which could be isolated by re-precipitation from ethanol by CH_2Cl_2.

Only one chemical form was found in the solution in the case of 1,2,3-triazole compounds in which the ligand is coordinated by the nitrogen atom in position 1 when examining both one-dimensional and two-dimensional spectra (Fig. 1, S7-S12).
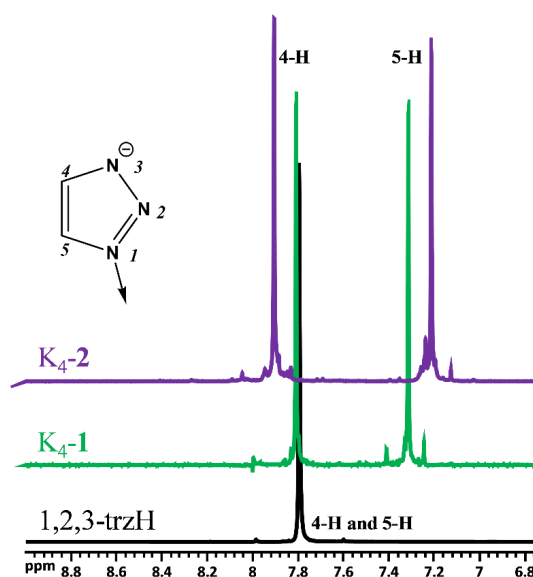

Figure 1. Fragment of ¹H NMR spectra of K₄-**1** and K₄-**2** in comparison with 1,2,3-triazole in DMSO-d₆.

Results and Discussion

Synthesis and characterization of cluster complexes

2

However, it is difficult to assign signals of the first and second nitrogen atoms. The assignment given in Figure 1 is based on the assumption that the influence of the cluster nucleus has a de-shielding effect and affects the first coordinated nitrogen atom to a greater extent, displacing the corresponding NMR peak to a weaker field. Upon coordination the position of the signal from hydrogen atom 5-H (i.e. the closest to the coordinating atom of nitrogen) is shifted upfield from 7.795 ppm to 7.311 or 7.210 ppm for Q = S or Se, respectively (Fig. 1).

In contrast, the spectra of K_4-**3** and K_4-**4** are far more complicated (Fig. 2, S13-S20). Various forms of complexes were found in the solution, which differ in the coordination of the ligand. The composition of the complexes can be described by the general formula $K_4[\{Re_6Q_8\}(1,2,4\text{-trz})^{type^I}{}_n(1,2,4\text{-trz})^{type^{II}}{}_{6-n}]$, where type[I] is the ligand coordinated by the nitrogen atom in the first position of the heterocycle, type[II] – is in the fourth position. According to this it can be calculated that, in general, up to 10 isomers are possible. The assignment of nitrogen atoms was carried out on the basis of changes in chemical shifts in comparison with free 1,2,4-triazole.[12] According to [13], non-coordinating nitrogen atoms in the 1,2,4-triazole fragment and practically do not change their position in comparison to the chemical shifts in the free ligand. For type[II] ligands, it was only possible to observe a signal of one 4-N atom. Most likely, this is due to the process of tautomeric exchange, which results in 1-N and 2-N atoms being equivalent to each other and thus not appearing in the two-dimensional spectrum.
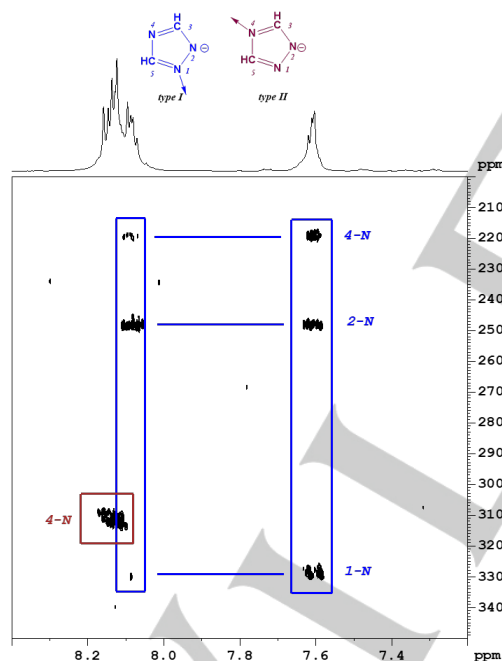

Figure 2. ^{1}H,^{15}N-NMR HMBC spectrum of K_4-**1** in DMSO-d_6.

The assignment of signals in the ^{1}H and ^{13}C spectra is based on two-dimensional C, H and N, H correlations (Fig. S17-S20). One can say that in both cases following the integrated signal intensities, the proportion of coordinated ligands of type[II] is slightly dominant and equal to 55% and 58% for Q = S and Se, respectively. The dominancy of type[II] ligand in the NMR signifies that nitrogen atom in position 4 is a stronger nucleophile, despite the fact that type[I] ligand should statistically appear twice as

frequently due to equivalency of nitrogen atoms in the position 1 and 2. On the other hand, the fact of presence of complexes with type[I] ligands in the NMR suggests that coordination reaction is irreversible, while the formation of the complexes is controlled by kinetics.

The results obtained from mass-spectroscopy are also in the agreement with the suggested molecular formula: namely the spectra of all four compounds feature signals that contain forms with six triazole ligands as well as daughter species with the number of apical ligands below 6 (Fig. S21-S24).

Crystallographic studies

For the 1,2,3-triazole compounds, we managed to attain crystals and to determine three single crystal structures. Namely K_4-**1**·6(1,2,3-trzH)·4H$_2$O, K_4-**2**·6(1,2,3-trzH), obtained directly from the reaction mixture before purification and Na$_4$-**1**·4EtOH·10H$_2$O obtained after the purification. For ions **3** and **4**, no crystal compounds were obtained, which is likely to be due to the presence of a high variety of structural and geometric isomers.

Compound K_4-**1**·6(1,2,3-trzH)·4H$_2$O contains the anions $[\{Re_6S_8\}(1,2,3\text{-trz})_6]^{4-}$ predicted by NMR (Fig. 3a). Terminal triazole ligands in *trans* positions form chains *via* solvate water molecules and potassium cations, where N…K contacts are 2.79 Å and O...K contacts are 2.64–2.81 Å (Fig. S25a). These potassium cations are also involved in the interaction with four solvate 1,2,3-triazole molecules through N…K (2.80 Å) and C-H…K (C…K 3.04 Å) contacts. Such chains are connected by N-H…N hydrogen bonds between two another 1,2,3-triazole ligands and solvate 1,2,3-triazole molecules in chains (N…N distance is 2.82 Å) (Fig. S25b). The remaining two terminal ligands are also involved in N-H…N hydrogen bonds with the two remaining solvate triazole molecules (N…N distance is 2.78 Å). In contrast to K_4-**1**·6(1,2,3-trzH)·4H$_2$O, cluster anions in K_4-**2**·6(1,2,3-trzH) are connected with each other *via* solvate molecules of 1,2,3-triazole and potassium cations (Fig. S26). These interactions can be described as a distorted K_8 cube connected with six apical 1,2,3-triazole ligands from six different cluster anions through N…K contacts (2.88 Å) and six solvate 1,2,3-triazoles through N...K (3.03–3.12 Å) and C-H…K (C…K 2.97–3.12 Å) contacts.
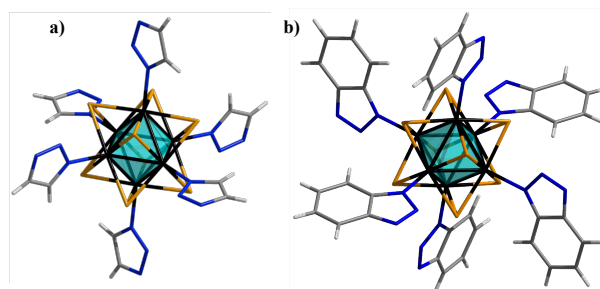

Figure 3. (a) The structure of $[\{Re_6Q_8\}(1,2,3\text{-trz})_6]^{4-}$ (b) The structure of $[\{Re_6Q_8\}(btrz)_6]^{4-}$ is given for comparison.

In the structure of Na$_4$-**1**·4EtOH·10H$_2$O, the cluster anions **1** are connected by complex chain-like cations $[(EtOH)Na(\mu\text{-}H_2O)_3Na(EtOH)(\mu\text{-}H_2O)_2Na(EtOH)(\mu\text{-}H_2O)_3Na(EtOH)]^{4+}$ (Na…OH$_2$ 2.35-2.40 Å, Na…OEt 2.32–2.39 Å, Na…S 2.83 Å, Na…N 2.48 Å) (Fig. S27). The chains are also connected *via* hydrogen bonds between H$_2$O molecules of the complex cation and the organic ligands where the N…O distances are equal to

3

2.92 Å. The voids between the chains are filled with 2 molecules of H_2O per formula unit.

Optical and electrochemical properties

The luminescent properties of compounds K_4-**1**-**4** were characterized in the solid state and in deaerated aqueous solutions, since the luminescence of octahedral clusters quenches well with molecular oxygen. The emission spectra and the luminescence decay profiles are given in Fig S28-S35, while the photophysical characteristics: emission maximum wavelengths (λ_{em}), emission lifetimes (τ_{em}) and quantum yields (Φ_{em}) in Table 2.

Table 2. Spectroscopic and photophysical parameters of compounds K_4-**n** (n = 1, 2, 3, 4) in comparison with literature data for K_4-**5** and K_4-**6**.

	K_4-**1**	K_4-**2**	K_4-**3**	K_4-**4**	K_4-**5**[a]	K_4-**6**[a]
			Solid state			
λ_{max}, nm	645	667	650	659	700	700
Φ	0.15	0.06	0.20	0.23	0.075	0.083
τ, μs	7.4	9.1	8.2	9.8	7.6, 2.9	7.7, 1.8
			Deaerated H_2O solution, pH=7			
λ_{max}, nm	650	660	645	655	705	700
Φ	<0.01	<0.01	<0.01	0.03	0.014	0.018
τ, μs	6.6	8.5	5.8	3.8	2.6	3.4
			Deaerated H_2O solution, pH=9			
λ_{max}, nm	650	660	646	657	–	–
Φ	<0.01	0.01	<0.01	0.03	–	–
τ, μs	5.9	8.4	7.2	3.2	–	–
			Deaerated D_2O solution, pH=7			
λ_{max}, nm	650	660	650	659	–	–
Φ	0.07	0.04	0.02	0.05	–	–
τ, μs	22.6	11.8	21.9	9.0	–	–

[a] from [4b], the data in H_2O soliton was at pH>6

Overall, the luminescent properties of the triazole complexes are similar to those reported for the benzotriazole analogues and other related compounds.[4b, 11] One can note from the data that the emission profile of the compounds is mostly dependent on the nature of the core rather than ligand. This is because the emission in the octahedral clusters originates from the triplet excited state, which is cluster core centered with only input from apical ligands orbitals.[14] This weak contribution of the ligands in the orbital was also confirmed by measurements of luminescence at different pH values (at pH=7 and pH=9): although the ligands, being weak bases, do participate in the acid-base equilibria, no difference in fluorescence was found. Unfortunately, solution experiments at acidic pH were impossible due to poor solubility of the compounds in acidic medium. Notably the luminescence quantum yield measured in deaerated H_2O solutions are noticeably smaller than that in the solid state, although the lifetimes are comparable. We believe that the reduction of Φ_{em} in aqueous medium is due to luminescence quenching via non-radiative energy transfer to H_2O vibrations in water molecules.[3b] Indeed, experiments undertaken in deaerated D_2O lead to a noticeable increase of both the photoluminescence quantum yield values and the lifetimes values.

The oxidation of compounds K_4-**1**-**6** was recorded in DMSO against an Ag/AgCl electrode. Figure 4 demonstrates the cyclic voltammogram of the compounds, while Table S1 summarizes the oxidation and reduction potentials. All complexes undergo a reversible one-electron oxidation, to give 23ē cluster species. In a similar manner to the luminescence properties, the potentials are only slightly dependent on the nature of the apical ligands and mostly are determined by the nature of the cluster core: selenium cluster complexes are more prone to oxidation than the sulfur analogues, for which the potentials are ~0.2 V higher. This behavior is rather typical for octahedral 24ē metal clusters and it signifies the decrease of the energy of HOMO orbital with the decrease of electronegativity of the inner ligand,[1b, 15] since this orbital is also mostly constituted from orbitals of the cluster core. It should be, however, noted that in the case of anions **2** and **4** the anodic peak is significantly broader and less defined. We presume this is due to the variety of isomers (observed by NMR spectroscopy) present in the solution, each with a slightly different oxidation potential. Apart from a one-electron oxidation, the cluster complexes also undergo a quasi-reversible reduction at ~ –0.75V, which is associated with the organic ligand-centered reduction. Such a reduction was described earlier for rhenium complexes with pyridine-based ligands or molybdenum complexes with 3,5-dinitrobenzoate.[16]
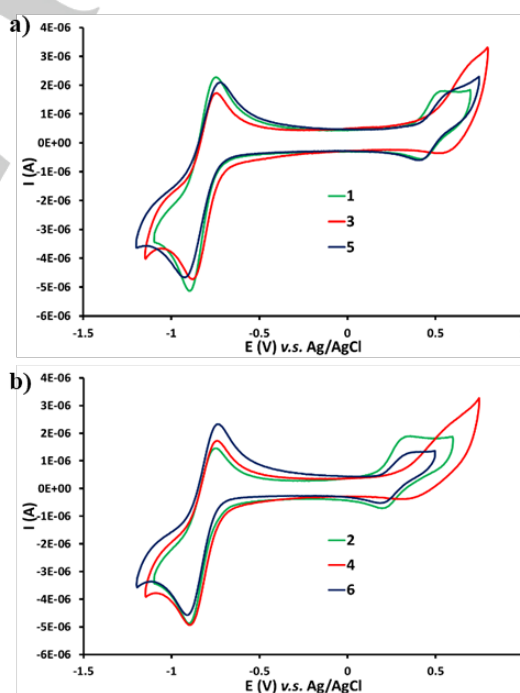

Figure 4. Cyclic voltammetry of the [{Re$_6$Q$_8$}L$_6$]$^{4-}$ (Q = S (a), Se (b)) anions (0.5 mM) in 0.1 M Bu$_4$NClO$_4$ DMSO solution.

Biological studies

The biological properties of the cluster anions **1**-**4** and the benzotriazole analogues **5**-**6** were studied using sodium salts rather the potassium to reduce the possible negative effect of the potassium ions, which will be paramount for any *in vivo* studies in

future. The toxicity profile was studied on cervical cancer cells (HeLa) and on the immortalized human fibroblasts (CRL-4025) cell line using the MTT assay and the results are presented in Figure 5, while values of IC_{50} are summarized in Table 3. According to our data, all six compounds had moderate toxicity to either of the cell lines with both of benzotriazole complexes being the most toxic from the lot.
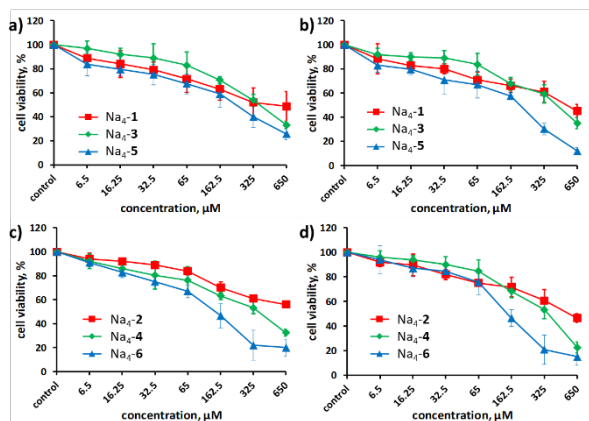

Figure 5. Cellular toxicity of Na₄-**n** detected by the MTT assay on HeLa (a,c) and CRL-4025 (b,d) cells.

Table 3. The IC_{50} of Na₄-**n** on the HeLa and CRL-4025 determined by the MTT assay

Compound	$IC_{50} \pm SEM$, µM	
	HeLa	CRL-4025
Na₄-**1**	370±30	550±30
Na₄-**2**	>650	540±70
Na₄-**3**	370±30	430±40
Na₄-**4**	380±10	350±20
Na₄-**5**	230±20 (123.7±0.8)[a]	190±10
Na₄-**6**	140±10 (122.6±0.2)[a]	160±10

[a] from [4b] for potassium salts on Hep-2 cells

The uptake of the cluster complexes by the cells was monitored by confocal microscopy and by flow cytometry. The distributions of the cells treated by the clusters according to their Flow scattering (FSC) vs the intensity of red luminescence (710 nm) are presented in Fig. S36. One can see that although the gated population sets in the case of the cells treated by Na₄-**1-6** were not identical with the control population set, the sets overlapped significantly and thus could not be easily distinguished. Therefore, the mean luminescence intensity per cell was calculated for the sake of comparison (Fig. 6). The data demonstrate that, indeed, both cell lines were on average statistically more luminescent than the control. However, the strongest difference in luminescence for the cells treated by the clusters was found in the case of Na₄-**6**,

which suggests that this complex was taken by the cells more efficiently. The confocal microscopy was performed for investigation of intracellular distribution of clusters. For the experiment both cell lines were incubated with 0.65 mM solutions of the clusters for 24 h and analyzed by confocal microscope under excitation at 405 nm and emission detection at 650-700 nm and the results are presented at the Figure 7 and S37. According to confocal images all of the cluster complexes, in particular for Na₄-**6**, entered the cancer cell line better than the fibroblasts. Moreover, as one can see both Na₄-**5** and Na₄-**6** also penetrated efficiently into the nucleus, which may explain the increased cytotoxicity of these complexes. In contrast, with the exception to Na₄-**6**, the red luminescence from fibroblasts was significantly less pronounced. It should also be noted that the character of emission from the cells treated by the benzotriazole complexes is visually different from that of triazole complexes: it is rather evenly distributed within the nucleus and perinuclear region, while emission from triazole complexes appears in punctate manner in the cytoplasm, which may suggest precipitation/aggregation of clusters onto or within the cells.
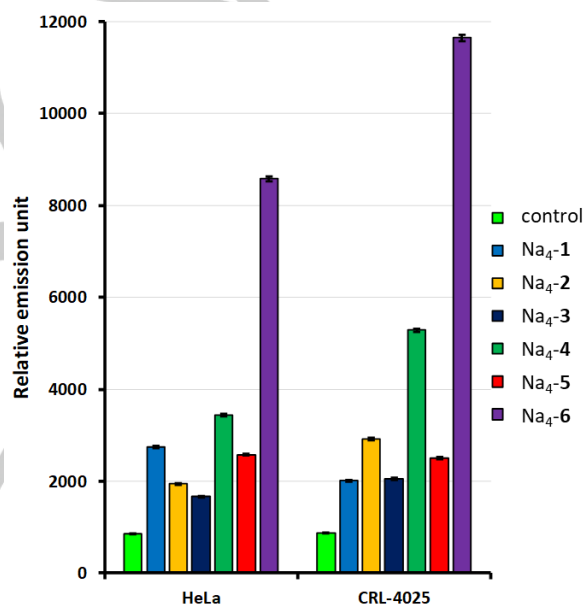

Figure 6. The uptake of the cluster complexes by HeLa and CRL-4025 cell lines, expressed as a relative emission unit (REU±SEM).

Having determined that cluster anions **5** and **6** do have preferential localization in nucleus we were interested to understand whether they also able to bind to DNA. We first attempted to evaluate the interaction between the clusters and DNA by electrophoresis. Clusters at concentration of 0.04 µM were incubated with plasmid DNA at 37° for 24 h followed by electrophoresis. The results are presented at Fig. S38. As one can see there is no clear change between pure DNA and DNA with cluster, which means even if there are interaction between the complexes and DNA, they are week.
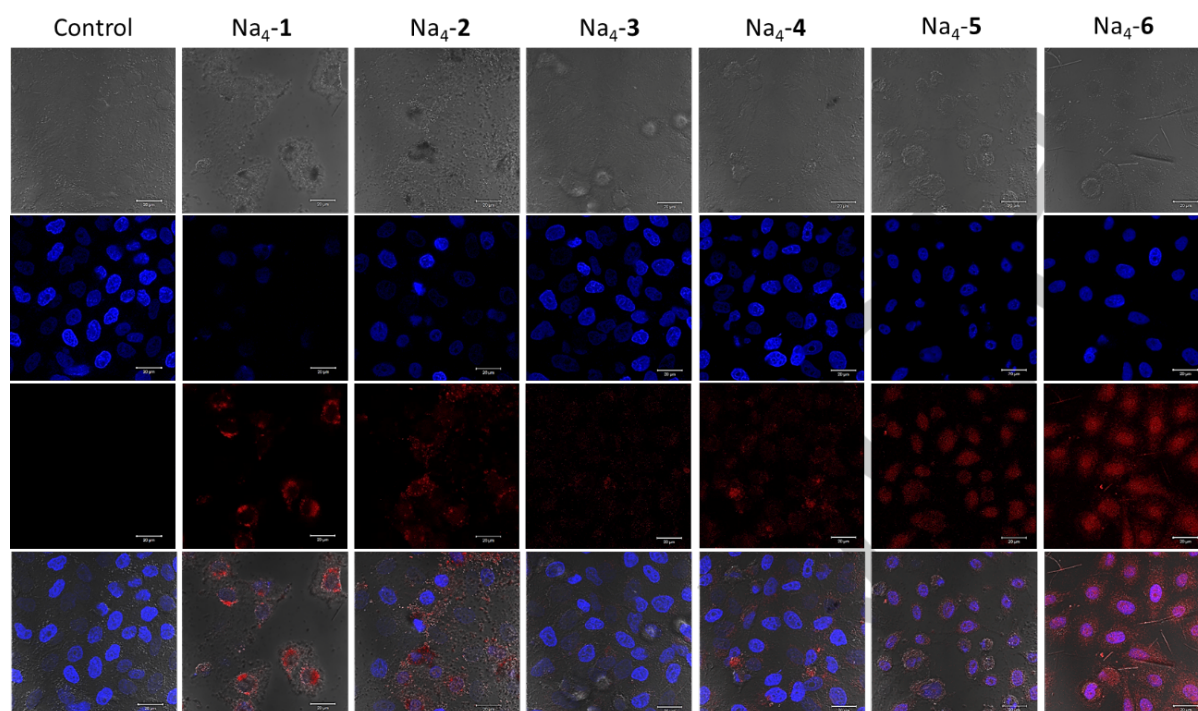
5

Figure 7. Intracellular distribution of clusters in HeLa cell line. Cell nuclei are colored by DAPI (blue), the luminescence of clusters is red.
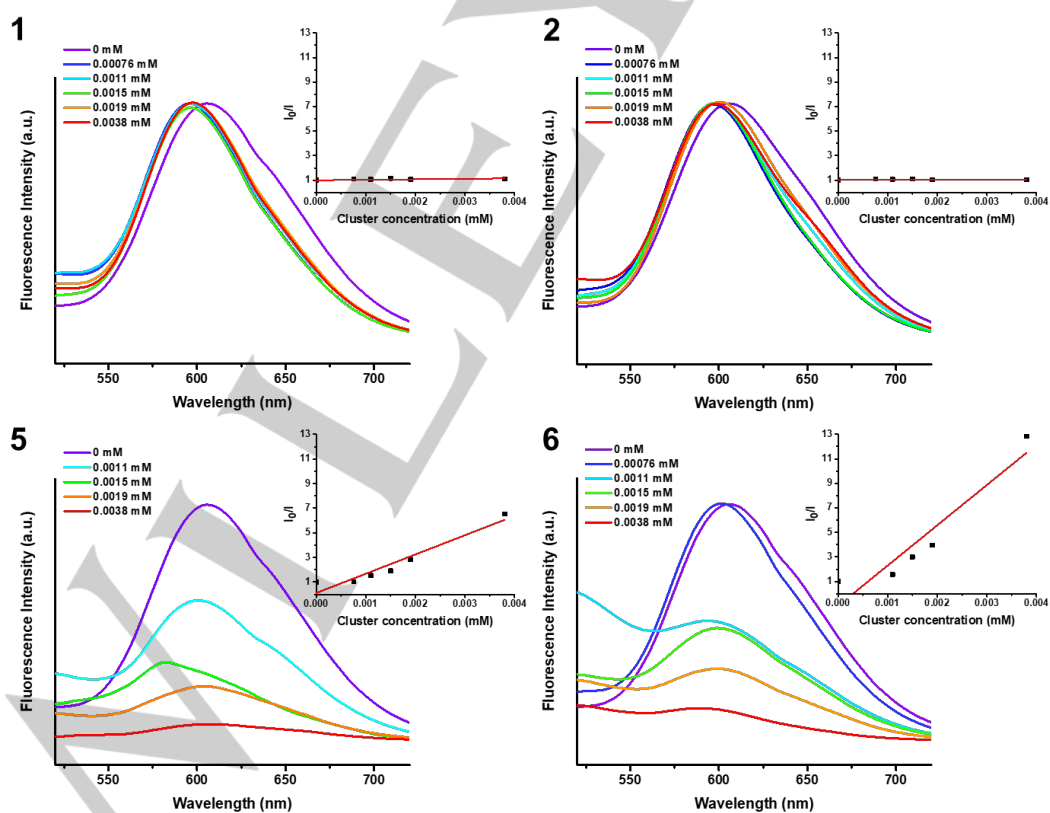

Figure 8. Effect of the rhenium cluster anions **1**, **2**, **5** and **6** on the fluorescence emission of the EB-*ct*DNA complex.

We than attempted fluorescence-based measurements as they should have higher sensitivity. It is known that Ethidium Bromide (EB) emits intense fluorescence in the presence of *ct*DNA, due to its strong intercalation between the adjacent *ct*DNA base pairs.[17] The quenching of the fluorescence of EB/*ct*DNA mixture in the presence of moieties capable to bind to *ct*DNA can be used to determine the extent of binding between the second molecule and *ct*DNA. The competitive binding experiments were carried out in TRIS buffer by keeping [DNA]:[EB] = 10:1 and varying the concentrations of Na4-**1**, Na4-**2**, K4-**5** and K4-**6** between 0 and 3.8×10^{-2} mM, where the upper limit of the cluster concentration in the experiment was established by undertaking a separate set of experiments in the absence of ctDNA (see below). The fluorescence spectra of EB were measured between 520 and 720 nm using an excitation wavelength of 405 nm and the emission range was set. The spectra were analyzed according to the classical Stern–Volmer Equation:

$$\frac{I_0}{I} = 1 + K_{SV} C$$

where I_0 and I are the integrated fluorescence intensities in the absence and presence of the quencher, respectively, K_{sv} is the linear Stern–Volmer quenching constant, C is the concentration of the quencher. The emission spectra and the Stern-Volmer plots are presented in Figure 8. As one can see, the 1,2,3-triazole containing clusters (**1** and **2**) exhibited insignificant binding affinity to *ct*DNA. This contrasted substantially by the btrz-containing clusters (**5** and **6**), which did show an interaction with *ct*DNA, as evidenced by the decrease in fluorescence intensity of the solutions. The Stern-Volmer constants (K_{SV}) for **5** and **6** were equal to $(1.6 \pm 0.2) \times 10^3$ mM^{-1} and $(3.3 \pm 0.6) \times 10^3$ mM^{-1}, respectively. These data show that the DNA binding affinity for **6** is almost twice as effective as that of **5**, indicating that not only the apical ligands but also the inner ligands may play a role in binding to DNA. The enhanced binding of the selenium cluster **6** to DNA also explains the enhanced accumulation of this compound in nucleus observed by confocal.

To confirm that the results are really due to interaction of the clusters with DNA we also undertook blank experiments in the absence of ctDNA (Figures S39) At concentrations of clusters **5** and **6** from 3.8×10^{-2} mM and above, the emission of EB (which in fact is significantly less intensive in the absence of DNA) started demonstrating some noticeable quenching (Fig. S39). This quenching with K_{SV} = 15±1 mM^{-1} for both complexes is an indication of some sort of interaction of clusters with EB, which is, however, weaker than the interaction of the clusters with ctDNA.
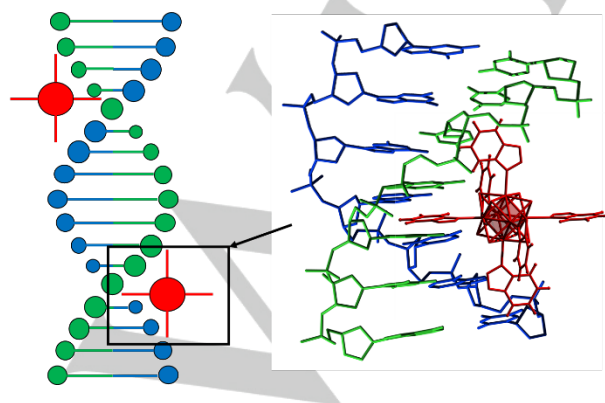

Figure 9. Schematic representation of suggested interaction of DNA with rhenium clusters.

Whilst the exact mechanism of binding to DNA is not uncovered, a plausible explanation for the affinity of the btrz clusters over 1,2,3-triazole ones could be the interaction of significantly larger aromatic system of benzotriazole with the nucleotide bases e.g. π-π stacking that would enhance DNA intercalation. Indeed, this mechanism was suggested earlier in the design of benzotriazole or benzimidazole based organic molecules and metal complexes with antibacterial, antifungal and anticancer activity.[18] To understand the role of the clusters in binding to DNA, free benzotriazole alone, was tested in the competitive binding experiments. Our data suggest that benzotriazole does indeed bind to DNA, but significantly less effectively than the clusters: for comparison K_{SV} = 3.9±0.7 mM^{-1} (Fig. S40) for binding of benzotriazole to DNA, i.e. it is three orders of magnitude lower than that for **5** and **6**. This experiment demonstrated the significant role of the cluster core in facilitating of binding of the cluster complexes **5** and **6** to DNA. We suggest that metal cluster provides effective orientational scaffolding for benzotriazole ligands, which facilitates binding of the clusters to DNA (Fig. 9).

Conclusion

In summary, we synthesized and characterized four new water-soluble anionic rhenium cluster complexes baring 1,2,3-triazole and 1,2,4-ligands. The complexes with [{Re6Q8}(1,2,3-trz)6]$^{4-}$ crystalize as a single geometric isomer, while [{Re6Q8}(1,2,4-trz)6]$^{4-}$ represents a mixture of a range of geometric isomers. The study of optical and electro-chemical properties demonstrated that the complexes with the same inner ligands are generally similar from the point of view of electronic structure to their benzotriazole analogues [{Re6Q8}(btrz)6]$^{4-}$. The study of biological properties revealed that despite the negative charge of the complexes internalization of the complexes with benzotriazole into HeLa and fibroblasts was better than those with triazole ligands. Moreover, the localization of the benzotriazole complexes within the cells' nucleus region suggested that there could be binding of with DNA. This assumption was indeed supported by the DNA binding test using EB as a marker. Notably, complexes with triazoles did not demonstrate any binding to free DNA. Our study, therefore, indeed confirmed that the presence of such hydrophobic, but π-rich unit as benzene ring is a driving force for the rhenium complexes cellular internalization.

Experimental Section

Materials and Methods

K4[{Re6Q8}(OH)6]·8H2O (Q = S, Se) was obtained according to the literature procedure.[7b] Na4[{Re6Q8}(OH)6] was synthesized from [{Re6Q8}(H2O)4(OH)2] according to the procedure described recently,[10] while compounds K4[{Re6S8}(btrz)6]·3.5EtOH·4H2O (K4-**5**) and K2.75H1.25[{Re6Se8}(btrz)6]·3EtOH·7H2O (K4-**6**) according to the method described in [4b]. All other reactants and solvents were purchased from Fisher, Alfa Aesar and Sigma-Aldrich and used as received. Elemental analyses were obtained using a EuroVector EA3000 Elemental Analyser. FTIR spectra (Fig. S41-S43) were recorded on a Bruker Vertex 80 as KBr disks. Energy-dispersive X-ray spectroscopy (EDS) was performed on a Hitachi TM3000 TableTop SEM with Bruker QUANTAX 70 EDS equipment. Absorption spectra were recorded on a Cary 60 UV-Vis

Spectrophotometer (Agilent). The high-resolution electrospray mass spectrometric (HR-ESI-MS) detection was performed at the Center of Collective Use «Mass spectrometric investigations» SB RAS in negative mode within 500-3000 m/z range on an electrospray ionization quadrupole time-of-filght (ESI-q-TOF) high-resolution mass spectrometer Maxis 4G (Bruker Daltonics, Germany). The 1D and 2D NMR spectra were recorded from a DMSO-d^6 solution at room temperature on a Bruker Avance III 500 FT-spectrometer with working frequencies 500.03, 125.73 and 50.67 MHz, for ^{1}H, ^{13}C, and ^{15}N nuclei, respectively. The ^{1}H and ^{13}C NMR chemical shifts are reported in ppm of the δ scale and referred to signals of the solvents (2.50 ppm for residual protons for ^{1}H and 39.50 ppm for ^{13}C NMR spectra respectively). ^{15}N NMR spectrum was obtained as projection of 2-D ^{1}H - ^{15}N - correlation. The ^{15}N NMR chemical shifts are referred to external standard of formamide (δ (^{15}N) = 112.5 ppm). Assignment of the signals were carried out using 2-D (HSQC, HMBC, COSY) NMR techniques.

Synthetic procedures

Syntheses of K$_4$[{Re$_6$S$_8$}(1,2,3-trz)$_6$]·EtOH (K$_4$-1) and K$_4$[{Re$_6$Se$_8$}(1,2,3-trz)$_6$]·EtOH·2H$_2$O (K$_4$-2). K$_4$[{Re$_6$Q$_8$}(OH)$_6$]·8H$_2$O (200 mg, 0.112 mmol (Q = S) or 0.092 mmol (Q = Se)) and 1,2,3-trzH (200 mg, 2.897 mmol) were heated in a sealed glass tube at 200 ºC for 2 days. After that tubes were opened and the reaction mixtures were dissolved in ethanol (30 mL) under heating. Solutions obtained were filtered from unreacted cluster, evaporated to around 5 mL and precipitated by excess of ethyl acetate. The resulted powders usually contain solvate 1,2,3-triazole molecules, which can be removed by few extra steps: conversion of the salt into the neutral water-insoluble [{Re$_6$Q$_8$}(1,2,3-trzH)$_4$(1,2,3-trz)$_2$] with the help of 1M HCl, followed by the conversion of the neutral complex back into the salt by KOH into ethanol and finally recrystallisation from DMSO by precipitation of the neat product with ethyl acetate. As assessed by CHNS analysis the product sometimes contained 1-2 molecules of DMSO per formula unit, which could be isolated by re-precipitation from ethanol by CH$_2$Cl$_2$. The final products were dried in air.

K$_4$-**1**: 170 mg (72 %), Anal. Calcd. for C$_{14}$H$_{18}$K$_4$N$_{18}$ORe$_6$S$_8$: C, 8.5; H, 0.9; N, 12.7; S, 12.9. Found: C, 8.6; H, 0.8; N, 12.4; S, 12.8. EDS: Re:S:K atomic ratio was equal to 6:8.1:3.8. ^{1}H NMR (500 MHz, DMSO) δ 7.31 (s, 1H, 5-CH), 7.81 (s, 1H, 4-CH). ^{13}C NMR (126 MHz, DMSO) δ 129.39 (5-C), 139.01 (4-C). ^{15}N NMR (51 MHz, HCONH$_2$) δ 252 (3-N), 350 (2-N), 396 (1-N). HR-ESI-MS (–): 593.8857 ({[{Re$_6$S$_8$}(1,2,3-trz)$_6$]}$^{3-}$), 820.8022 ({[{Re$_6$S$_8$}(1,2,3-trz)$_4$]}$^{2-}$), 856.8146 ({[{Re$_6$S$_8$}(1,2,3-trz)$_5$]}$^{2-}$), 876.2964 ({K[{Re$_6$S$_8$}(1,2,3-trz)$_5$]}$^{2-}$), 929.7906 ({K$_2$[{Re$_6$S$_8$}(1,2,3-trz)$_6$]}$^{2-}$). The TGA analysis indicated stability up to 180 °C with a weight loss of approximately 2.4% between 40 and 110 °C (the theoretical weight loss of EtOH is 2.3%) (Fig. S44). The single crystals of K$_4$-**1**·6(1,2,3-trzH)·4H$_2$O suitable for X-ray structural analyses were separated manually from the melts.

K$_4$-**2**: 180 mg (80 %), Anal. Calcd. for C$_{14}$H$_{22}$K$_4$N$_{18}$O$_3$Re$_6$Se$_8$: C, 7.0; H, 0.9; N, 10.5. Found: C, 7.2; H, 0.9; N, 10.3. EDS: Re:Se:K atomic ratio was equal to 6:8.2:3.9. ^{1}H NMR (500 MHz, DMSO) δ 7.21 (s, 1H, 5-CH), 7.90 (s, 1H, 4-CH). ^{13}C NMR (126 MHz, DMSO) δ 128.85 (5-C), 141.62 (4-C). ^{15}N NMR (51 MHz, HCONH$_2$) δ 245 (3-N), 348 (2-N), 402 (1-N). HR-ESI-MS (–): 719.0724 ({[{Re$_6$Se$_8$}(1,2,3-trz)$_6$]}$^{3-}$), 1010.5829 ({[{Re$_6$Se$_8$}(1,2,3-trz)$_4$]}$^{2-}$), 1044.5954 ({[{Re$_6$Se$_8$}(1,2,3-trz)$_5$]}$^{2-}$), 1065.0770 ({K[{Re$_6$Se$_8$}(1,2,3-trz)$_5$]}$^{2-}$), 1098.0897 ({K[{Re$_6$Se$_8$}(1,2,3-trz)$_6$]}$^{2-}$), 1118.5713 ({K$_2$[{Re$_6$S$_8$}(1,2,3-trz)$_6$]}$^{2-}$). The TGA analysis indicated stability up to 180°C with a weight loss of approximately 3.5% between 40 and 120°C (the theoretical weight loss of EtOH and 2H$_2$O is 3.4%) (Fig. S44). The single crystals of K$_4$-**2**·6(1,2,3-trzH) suitable for X-ray structural analyses were separated manually from the melts.

Syntheses of K$_4$[{Re$_6$S$_8$}(1,2,4-trz)$_6$]·2EtOH·3H$_2$O (K$_4$-3) and K$_4$[{Re$_6$Se$_8$}(1,2,4-trz)$_6$]·EtOH·3H$_2$O (K$_4$-4). Compounds were obtained using same procedure as for K$_4$-**1** and K$_4$-**2** from K$_4$[{Re$_6$Q$_8$}(OH)$_6$]·8H$_2$O (200 mg, 0.112 mmol (Q = S) or 0.092 mmol (Q = Se)) and 1,2,4-trzH (200 mg, 2.897 mmol).

K$_4$-**3**: 190 mg (81 %), Anal. Calcd. for C$_{16}$H$_{30}$K$_4$N$_{18}$O$_5$Re$_6$S$_8$: C, 9.2; H, 1.4; N, 12.1; S, 12.3. Found: C, 9.1; H, 1.5; N, 12.2; S, 12.5. EDS: Re:S:K atomic ratio was equal to 6:7.9:3.9. ^{1}H NMR (500 MHz, DMSO) δ 7.56-7.67 (m, 1H, 5-H for the type I), 8.00-8.10 (m, 1H, 3-H for the type I), 8.10-8.22 (m, 2.46H, 3,5-H for the type II). ^{13}C NMR (126 MHz, DMSO) δ 151.50-150.60 (3-C for the type I), 155.29-155.36 (3,5-C for the type II), 158.44-158-64 (5-C for the type I). ^{15}N NMR (51 MHz, HCONH$_2$) δ 219 (4-N for the type I), 248 (2-N for the type I), 312 (4-N for the type II), 329 (1-N for the type I. HR-ESI-MS (–): 593.8849 ({[{Re$_6$S$_8$}(1,2,4-trz)$_6$]}$^{3-}$), 820.8022 ({[{Re$_6$S$_8$}(1,2,4-trz)$_4$]}$^{2-}$), 856.8146 ({[{Re$_6$S$_8$}(1,2,4-trz)$_5$]}$^{2-}$), 857.3186 ({H[{Re$_6$S$_8$}(1,2,4-trz)$_5$]}$^{2-}$), 876.2964 ({K[{Re$_6$S$_8$}(1,2,4-trz)$_5$]}$^{2-}$), 929.7906 ({K$_2$[{Re$_6$S$_8$}(1,2,4-trz)$_6$]}$^{2-}$). The TGA analysis indicated stability up to 260 °C with a weight loss of approximately 6.9% between 50 and 200 °C (the theoretical weight loss of 2EtOH and 3H$_2$O is 7.0%) (Fig. S45).

K$_4$-**4**: 175 mg (78 %), Anal. Calcd. for C$_{14}$H$_{24}$K$_4$N$_{18}$O$_4$Re$_6$Se$_8$: C, 6.9; H, 1.0; N, 10.4. Found: C, 7.1; H, 0.8; N, 10.2. EDS: Re:Se:K atomic ratio was equal to 6:8.1:4.0. ^{1}H NMR (500 MHz, DMSO) δ 7.49-7.59 (m, 1H, 5-H for the type I), 8.00-8.20 (m, 1H, 3-H for the type I), 8.15-8.22 (m, 2.53H, 3,5-H for the type II). ^{13}C NMR (126 MHz, DMSO) δ 149.60-150.30 (3-C for the type I), 157.58-158.08 (3,5-C for the type II), 160.56-161.21 (5-C for the type I). ^{15}N NMR (51 MHz, HCONH$_2$) δ 213 (4-N for the type I), 248 (2-N for the type I), 308 (4-N for the type II), 336 (1-N for the type I). HR-ESI-MS (–): 719.0724 ({[{Re$_6$Se$_8$}(1,2,4-trz)$_6$]}$^{3-}$), 1010.5829 ({[{Re$_6$Se$_8$}(1,2,4-trz)$_4$]}$^{2-}$), 1044.5954 ({[{Re$_6$Se$_8$}(1,2,4-trz)$_5$]}$^{2-}$), 1064.0770 ({K[{Re$_6$Se$_8$}(1,2,4-trz)$_5$]}$^{2-}$), 1118.5713 ({K$_2$[{Re$_6$S$_8$}(1,2,4-trz)$_6$]}$^{2-}$). The TGA analysis indicated stability up to 260 °C with a weight loss of approximately 3.9% between 50 and 200 °C (the theoretical weight loss of EtOH and 3H$_2$O is 4.1%) (Fig. S45).

Syntheses of sodium salts of cluster complexes. Sodium salts Na$_4$[{Re$_6$S$_8$}(1,2,3-trz)$_6$]·EtOH·H$_2$O (Na$_4$-**1**), Na$_4$[{Re$_6$Se$_8$}(1,2,3-trz)$_6$]·2EtOH·2H$_2$O (Na$_4$-**2**), Na$_4$[{Re$_6$S$_8$}(1,2,4-trz)$_6$]·2EtOH·H$_2$O (Na$_4$-**3**) and Na$_4$[{Re$_6$Se$_8$}(1,2,4-trz)$_6$]·2EtOH·2H$_2$O (Na$_4$-**4**), Na$_4$[{Re$_6$S$_8$}(btrz)$_6$]·EtOH·2H$_2$O (Na$_4$-**5**), Na$_4$[{Re$_6$Se$_8$}(btrz)$_6$]·EtOH·2H$_2$O (Na$_4$-**6**) were prepared in the similar fashion the potassium salts, but using Na$_4$[{Re$_6$Q$_8$}(OH)$_6$] instead of K$_4$[{Re$_6$Q$_8$}(OH)$_6$].

Na$_4$-**1**: 162 mg (71 %), Anal. Calcd. for C$_{14}$H$_{20}$N$_{18}$Na$_4$O$_2$Re$_6$S$_8$: C, 8.7; H, 1.0; N, 13.0; S, 13.2. Found: C, 9.0; H, 0.9; N, 13.0; S, 12.9. EDS: Re:S:Na atomic ratio was equal to 6:8.0:3.8. The TGA analysis indicated stability up to 200 °C with a weight loss of approximately 3.0% between 50 and 170 °C (the theoretical weight loss of EtOH and H$_2$O is 3.3%) (Fig. S46). The single crystals of Na$_4$-**1**·4EtOH·10H$_2$O suitable for X-ray structural analyses were obtained by slow evaporation of ethanol solution.

Na$_4$-**2**: 168 mg (74 %), Anal. Calcd. for C$_{16}$H$_{28}$N$_{18}$Na$_4$O$_4$Re$_6$Se$_8$: C, 8.0; H, 1.2; N, 10.5. Found: C, 8.1; H, 1.1; N, 10.3. EDS: Re:Se:Na atomic ratio was equal to 6:7.8:3.8. The TGA analysis indicated stability up to 200 °C with a weight loss of approximately 5.6% between 50 and 170 °C (the theoretical weight loss of 2EtOH and 2H$_2$O is 5.4%) (Fig. S46).

Na$_4$-**3**: 185 mg (80 %), Anal. Calcd. for C$_{16}$H$_{26}$N$_{18}$Na$_4$O$_3$Re$_6$S$_8$: C, 9.7; H, 1.3; N, 12.7; S, 12.9. Found: C, 9.6; H, 1.2; N, 12.5; S, 12.7. EDS: Re:S:Na atomic ratio was equal to 6:8.0:4.2. The TGA analysis indicated stability up to 210 °C with a weight loss of approximately 5.4% between 50 and 160 °C (the theoretical weight loss of 2EtOH and H$_2$O is 5.5%) (Fig. S47).

Na$_4$-**4**: 171 mg (75 %), Anal. Calcd. for C$_{16}$H$_{28}$N$_{18}$Na$_4$O$_4$Re$_6$Se$_8$: C, 8.0; H, 1.2; N, 10.5. Found: C, 8.1; H, 1.0; N, 10.2. EDS: Re:Se:Na atomic ratio was equal to 6:7.8:3.9. The TGA analysis indicated stability up to 210 °C with a weight loss of approximately 5.4% between 50 and 160 °C (the theoretical weight loss of 2EtOH and 2H$_2$O is 5.4%) (Fig. S47).

Na$_4$-**5**: 224 mg (85 %), Anal. Calcd. for C$_{38}$H$_{34}$N$_{18}$Na$_4$O$_3$Re$_6$S$_8$: C, 20.2; H, 1.5; N, 11.1; S, 11.3. Found: C, 20.1; H, 1.6; N, 11.2; S, 11.6. EDS: Re:S:Na atomic ratio was equal to 6:8.1:4.1. ^{1}H NMR (500 MHz, DMSO) δ 7.04 (m, 2H, 5,6-CH), 7.73 (m, 1H, 4-CH), 8.09(m, 1H, 7-CH). ^{13}C NMR

(126 MHz, DMSO) δ 116.56 (4-C), 118.14 (7-C), 120.45 (5-C), 121.09 (6-C), 145.37 (3'-C), 146.80 (7'-C). The TGA analysis indicated stability up to 400 °C with a weight loss of approximately 3.9% between 50 and 160 °C (the theoretical weight loss of EtOH and $2H_2O$ is 3.7%) (Fig. S48).

Na_4-**6**: 212 mg (84 %), Anal. Calcd. for $C_{38}H_{34}N_{18}Na_4O_3Re_6Se_8$: C, 17.3; H, 1.3; N, 9.5. Found: C, 17.1; H, 1.4; N, 9.2. EDS: Re:Se:Na atomic ratio was equal to 6:7.8:4.0. ^1H NMR (500 MHz, DMSO) δ 7.01 (m, 2H, 5,6-CH), 7.69 (m, 1H, 4-CH), 8.08(m, 1H, 7-CH). ^{13}C NMR (126 MHz, DMSO) δ 116.48 (4-C), 118.71 (7-C), 120.17 (5-C), 120.22 (6-C), 145.41 (3'-C), 146.89 (7'-C). The TGA analysis indicated stability up to 400 °C with a weight loss of approximately 3.9% between 50 and 160 °C (the theoretical weight loss of EtOH and $2H_2O$ is 3.8%) (Fig. S48).

Crystallography

Single-crystal X-ray diffraction data for K_4-**1**·6(1,2,3-trzH)·$4H_2O$, K_4-**2**·6(1,2,3-trzH) and Na_4-**1**·4EtOH·$10H_2O$ were collected at 150 K (for K_4-**1**·6(1,2,3-trzH)·$4H_2O$ and Na_4-**1**·4EtOH·$10H_2O$) or 298 K (for K_4-**2**·6(1,2,3-trzH)) on a Bruker Nonius X8 Apex 4K CCD diffractometer fitted with graphite monochromatized MoKα radiation (λ = 0.71073 Å). Absorption corrections were made empirically using the SADABS program.[19] The structures were solved by the direct method and further refined by the full-matrix least-squares method using the SHELXTL program package.[19] All non-hydrogen atoms were refined anisotropically. Table S2 summarizes crystallographic data, while CCDC 1994828-1994830 contain the supplementary crystallographic data for this paper. These data can be obtained free of charge from the Cambridge Crystallographic Data Centre via www.ccdc.cam.ac.uk/data_request/cif.

Photoluminescence measurements

Fluoromax-4 spectrofluorometer equipped with 150 W ozonefree Xe arc-lamp, R928P photomultiplier tube, integrating sphere Quanta-φ and double grating excitation and emission monochromators was used for luminescence characterization such as absolute quantum yield, luminescence life-times and emission profiles. Emission spectra were corrected for source intensity (lamp and grating) and emission spectral response (detector and grating) by standard correction curves. Powdered samples of the complexes Na_4-**1**, Na_4-**2**, Na_4-**3** and Na_4-**4** were placed in non-fluorescent quartz cuvettes. Emission spectra in solution were measured in either H_2O or D_2O in quartz cuvettes. The absorbance of solutions was set at < 0.1 at 355 nm. The solutions were deaerated by purging the cuvettes with nitrogen gas for 30 min and sealed. Corrected emission spectra were recorded at 355 nm excitation.

Cyclic Voltammetry

Cyclic voltammetry was carried out with Elins P-20X8 voltammetry analyzer using three-electrode scheme with Pt working, GC auxiliary and Ag/AgCl/3.5M KCl reference electrodes. Investigations were carried out for $5·10^{-4}$ M solutions of corresponding cluster compounds in 0.1 M Bu_4NClO_4 in DMSO under Ar atmosphere. The registered value of $E_{1/2}$ for $Fc^{0/+}$ couple was 0.405 V in the same conditions.

Cell culture

Cervical cancer cells HeLa (HeLa, CCL-2) and immortalized human fibroblasts (CRL-4025) was purchased from the American Type Culture Collection (USA) and cultured in DMEM supplemented with 10% fetal bovine serum, under a humidified atmosphere (5% CO_2 plus 95% air) at 37 °C.

MTT assay

MTT assay was performed according to standard procedures.[20] The cell cultures were grown on DMED containing 10% bovine serum. To each well

of a 96-well plate we added 100 μL of the cell suspension (density 10^6 cells/ml); the plate was placed in an incubator containing 5% CO_2 at a temperature of 37 ºC. After 24 h the test compounds were added in the required concentration. The plate was then returned to the incubator for a further 72 hours. Then, 10 μL of MTT (5 mg of 3-(4,5-dimethylthiazol-2-yl)-2,5-diphenyltetrazolium bromide (MTT) per 1 ml of PBS) was added to each well. 3 hours later the supernatant fluid was removed from the wells, and the precipitate was dissolved in 100 μL of isopropanol. The amount of precipitate was determined on a Multiskan RC plate spectrophotometer, using the inbuilt Genesis software (LabSystems). Percent inhibition was calculated by the formula:

Inhibition(%) = 100 – [(T/M)×100],

T is the optical density of the precipitate with the test compound, M is the optical density of the untreated cells (negative control). The experiment was repeated independently three times, with 3 replications in each. Average values were reported for all repeated experiments±SEM

Flow cytometry

Flow cytofluorimetry was performed using an AttuneNxT instrument (ThermoFisher Scientific). For this analysis, cells were seeded in the wells of a 6-well plate ($5×10^4$ cells per well) and incubated for 24 hours to attach. Then the test compounds were added in the required concentration. Cells were incubated for 24 hours, after this, cells from the wells were removed using trypsin and washed twice with 1 ml PBS. After the second wash, the cells were suspended in 1 ml of PBS and then analyzed using a cytofluorimeter. The final result is presented in the form of the relative emission units (REU±SEM) in the analysis of at least 30,000 cells.

Confocal microscopy

The samples for confocal microscopy were prepared as follows: a cover slip was placed into the bottom of each well of a 12-well plate, 1 ml of cell culture medium and 100 μL of cell suspension (density 10^6 cell per ml) were then added to each well. The cells were incubated for 24 hours, and then washed with PBS. After that, to each well was added a sample of one of the clusters under test, dissolved in cell culture medium at the desired concentration. After 24 h of incubation the cover slips were removed from the plate, carefully washed with PBS and put into paraformaldehyde overnight. Subsequently, each coverslip was placed on a slide with antifade containing DAPI. The sample was dried with filter paper and the edges of the coverslips were sealed to the slides with lacquer. Microscopic examination was carried out with the help of an LSM 510 META (Carl Zeiss) confocal scanning microscope at the Center for Microscopic Analysis of Biological Objects of the Institute of Cytology and Genetics SB RAS. Standard filters were used for detection of clusters (405 nm for excitation and 650-700 nm for emission). The results were processed using Zen (Carl Zeiss) software.

Electrophoretic mobility shift assay

Plasmid pUC19 was provided by SybEnzyme (Novosibirsk, Russia). Clusters at concentration of 0.04 μM were incubated with plasmid DNA pUC19 (0.5 μg) at 37º for 24 h followed by electrophoresis (4 h at 100 V in 1.2% agarose TAE gel). Then the gel was staining with ethidium bromide and results were detected in UV.

Fluorescence titration

DNA sodium salt from calf thymus (*ct*DNA) was purchased from Sigma-Aldrich. Cluster compounds Na_4-**1**, Na_4-**2**, K_4-**5** and K_4-**6** were investigated for their ability to bind to DNA via displacement of EB from EB-*ct*DNA complexes. The tested solutions were prepared by mixing 2 mL of *ct*DNA (100 μg mL^{-1} in TRIS buffer solution) and 2 μL of EB solution (10 mg mL^{-1}) to which separate aliquots of 0, 20, 30, 40, 50 or 100 μL of the cluster

stock solutions (0.38 mM in DMSO) were added and made up to 10 mL using Tris-Buffer solution. The luminescence of the solutions was measured on a HORBIA Scientific fluormax-4 spectrofluorometer with a HORBIA DM303 current acquisition module between 520-720 nm using a 405 nm excitation source at room temperature. To study effect of benzotriazole on EB-*ct*DNA, aliquots of a stock solution of benzotriazole (2.28 mM in TRIS buffer solution) equal to 0, 20, 40, 100 μL were used. To study influence of clusters on EB luminescence, the same concentrations of EB were studied, but with the addition of other aliquots of cluster stock solution (100, 200, 500, and 1250 μL). Luminescence was detected at 550–750 nm upon excitation with a wavelength of 520 nm in order to exclude the effect of luminescence of the cluster complexes.

Acknowledgements

[1] a) N. Kitamura, Y. Ueda, S. Ishizaka, K. Yamada, M. Aniya, Y. Sasaki, *Inorg. Chem.* **2005**, *44*, 6308–6313; b) T. Yoshimura, S. Ishizaka, Y. Sasaki, H.-B. Kim, N. Kitamura, N. G. Naumov, M. N. Sokolov, V. E. Fedorov, *Chem. Lett.* **1999**, *28*, 1121-1122.

[2] A. A. Krasilnikova, A. O. Solovieva, A. A. Ivanov, K. E. Trifonova, T. N. Pozmogova, A. R. Tsygankova, A. I. Smolentsev, E. I. Kretov, D. S. Sergeevichev, M. A. Shestopalov, Y. V. Mironov, A. M. Shestopalov, A. F. Poveshchenko, L. V. Shestopalova, *Nanomedicine: NBM* **2017**, *13*, 755-763.

[3] a) L. Gao, M. A. Peay, T. G. Gray, *Chem. Mater.* **2010**, *22*, 6240-6245; b) A. O. Solovieva, K. Kirakci, A. A. Ivanov, P. Kubát, T. N. Pozmogova, S. M. Miroshnichenko, E. V. Vorontsova, A. V. Chechushkov, K. E. Trifonova, M. S. Fufaeva, E. I. Kretov, Y. V. Mironov, A. F. Poveshchenko, K. Lang, M. A. Shestopalov, *Inorg. Chem.* **2017**, *56*, 13491-13499.

[4] a) J. G. Elistratova, K. A. Brylev, A. O. Solovieva, T. N. Pozmogova, A. R. Mustafina, L. V. Shestopalova, M. A. Shestopalov, V. V. Syakayev, A. A. Karasik, O. G. Sinyashin, *J. Photochem. Photobiol. A* **2017**, *340*, 46-52; b) M. A. Shestopalov, K. E. Zubareva, O. P. Khripko, Y. I. Khripko, A. O. Solovieva, N. V. Kuratieva, Y. V. Mironov, N. Kitamura, V. E. Fedorov, K. A. Brylev, *Inorg. Chem.* **2014**, *53*, 9006-9013.

[5] O. A. Efremova, K. A. Brylev, O. Kozlova, M. S. White, M. A. Shestopalov, N. Kitamura, Y. V. Mironov, S. Bauer, A. J. Sutherland, *J. Mater. Chem. C* **2014**, *2*, 8630-8638

[6] a) F. Camerel, F. Kinloch, O. Jeannin, M. Robin, S. K. Nayak, E. Jacques, K. A. Brylev, N. G. Naumov, Y. Molard, *Dalton Trans.* **2018**, *47*, 10884-10896; b) Y. Molard, A. Ledneva, M. Amela-Cortes, V. Cîrcu, N. G. Naumov, C. Mériadec, F. Artzner, S. Cordier, *Chem. Mater.* **2011**, *23*, 5122–5130.

[7] a) N. G. Naumov, A. V. Virovets, Y. V. Mironov, S. B. Artemkina, V. E. Fedorov, *Ukr. Chem. J.* **1999**, *65*, 21-27; b) S. S. Yarovoi, Y. V. Mironov, D. Y. Naumov, Y. V. Gatilov, S. G. Kozlova, S.-J. Kim, V. E. Fedorov, *Eur. J. Inorg. Chem.* **2005**, *2005*, 3945-3949; c) H. Imoto, N. G. Naumov, A. V. Virovets, T. Saito, V. E. Fedorov, *J. Struct. Chem.* **1998**, *39*, 720-727; d) N. G. Naumov, A. V. Virovets, N. V. Podberezskaya, V. E. Fedorov, *J. Struct. Chem.* **1997**, *38*, 857-862.

[8] H. Lusic, M. W. Grinstaff, *Chem. Rev.* **2013**, *113*, 1641-1666.

[9] a) A. A. Ivanov, V. K. Khlestkin, K. A. Brylev, I. V. Eltsov, A. I. Smolentsev, Y. V. Mironov, M. A. Shestopalov, *J. Coord. Chem.* **2016**, *69*, 841-850; b) A. A. Ivanov, D. I. Konovalov, T. N. Pozmogova, A. O. Solovieva, A. R. Melnikov, K. A. Brylev, N. V. Kuratieva, V. V. Yanshole, K. Kirakci, K. Lang, S. N. Cheltygmasheva, N. Kitamura, L. V. Shestopalova, Y. V. Mironov, M. A. Shestopalov, *Inorg. Chem. Front.* **2019**, *6*, 882-892; c) A. A. Krasilnikova, M. A. Shestopalov, K. A. Brylev, I. A. Kirilova, O. P. Khripko, K. E. Zubareva, Y. I. Khripko, V. T. Podorognaya, L. V. Shestopalova, V. E. Fedorov, Y. V. Mironov, *J. Inorg. Biochem.* **2015**, *144*, 13-17; d) A. A. Krasilnikova, A. O. Solovieva, A. A. Ivanov, K. A. Brylev, T. N. Pozmogova, M. A. Gulyaeva, O. G. Kurskaya, A. Y. Alekseev, A. M. Shestopalov, L. V. Shestopalova, A. F. Poveshchenko, O. A. Efremova, Y. V. Mironov, M. A. Shestopalov, *Toxicol Res.* **2017**, *6*, 554-560.

[10] A. A. Krasilnikova, A. O. Solovieva, K. E. Trifonova, K. A. Brylev, A. A. Ivanov, S.-J. Kim, M. A. Shestopalov, M. S. Fufaeva, A. M. Shestopalov, Y. V. Mironov, A. F. Poveshchenko, L. V. Shestopalova, *Contrast Media Mol. Imaging* **2016**, *11*, 459-466.

[11] a) D. I. Konovalov, A. A. Ivanov, Y. A. Vorotnikov, K. A. Brylev, I. V. Eltsov, N. V. Kuratieva, N. Kitamura, Y. V. Mironov, M. A. Shestopalov, *Inorg. Chim. Acta* **2019**, *498*, 119128; b) D. I. Konovalov, A. A. Ivanov, Y. A. Vorotnikov, A. I. Smolentsev, I. V. Eltsov, O. A. Efremova, N. Kitamura, Y. V. Mironov, M. A. Shestopalov, *Polyhedron* **2019**, *165*, 79-85.

[12] R. M. Claramunt, C. López, D. Sanz, I. Alkorta, J. Elguero, *Heterocycles* **2001**, *55*, 2109-2121.

[13] I. Łakomska, K. Stefańczak, M. Fandzloch, J. Sitkowski, B. Filip-Psurska, A. Wojtczak, *Polyhedron* **2016**, *108*, 33-39.

[14] a) Z.-N. Chen, T. Yoshimura, M. Abe, K. Tsuge, Y. Sasaki, S. Ishizaka, H.-B. Kim, N. Kitamura, *Chem. Eur. J.* **2001**, *7*, 4447-4455; b) T. Yoshimura, A. Matsuda, Y. Ito, S. Ishizaka, S. Shinoda, H. Tsukube, N. Kitamura, A. Shinohara, *Inorg. Chem.* **2010**, *49*, 3473-3481; c) T. Yoshimura, K. Umakoshi, Y. Sasaki, S. Ishizaka, H.-B. Kim, N. Kitamura, *Inorg. Chem.* **2000**, *39*, 1765–1772.

[15] A. A. Ivanov, C. Falaise, P. A. Abramov, M. A. Shestopalov, K. Kirakci, K. Lang, M. A. Moussawi, M. N. Sokolov, N. G. Naumov, S. Floquet, D. Landy, M. Haouas, K. A. Brylev, Y. V. Mironov, Y. Molard, S. Cordier, E. Cadot, *Chem. Eur. J.* **2018**, *24*, 13467-13478.

[16] a) S. Fujii, T. Horiguchi, S. Akagi, N. Kitamura, *Inorg. Chem.* **2016**, *55*, 10259-10266; b) T. Yoshimura, K. Umakoshi, Y. Sasaki, A. G. Sykes, *Inorg. Chem.* **1999**, *38*, 5557-5564.

[17] a) S. Kathiresan, S. Mugesh, J. Annaraj, M. Murugan, *New J. Chem.* **2017**, *41*, 1267-1283; b) W. D. Wilson, L. Ratmeyer, M. Zhao, L. Strekowski, D. Boykin, *Biochemistry* **1993**, *32*, 4098-4104.

[18] a) Y. Ren, L. Zhang, C.-H. Zhou, R.-X. Geng, *Med. chem.* **2014**, *4*, 640-662; b) N. Ling, X. Wang, D. Zeng, Y.-W. Zhang, X. Fang, H.-X. Yang, *J. Mol. Struct.* **2020**, *1206*, 127641; c) G. Onar, C. Gürses, M. O. Karataş, S. Balcıoğlu, N. Akbay, N. Özdemir, B. Ateş, B. Alıcı, *J. Organomet. Chem.* **2019**, *886*, 48-56; d) G. Onar, M. O. Karataş, S. Balcıoğlu, T. T. Tok, C. Gürses, I. Kılıç-Cıkla, N. Özdemir, B. Ateş, B. Alıcı, *Polyhedron* **2018**, *153*, 31-40; e) H. Liu, L. Gopala, S. R. Avula, P. Jeyakkumar, X. Peng, C. Zhou, R. Geng, *Chin. J. Chem.* **2017**, *35*, 483-496.

[19] *Bruker, APEX2 (Version 1.08), SAINT (Version 07.03), SADABS (Version 02.11), SHELXTL (Version 06.12), Bruker AXS Inc., Madison, WI, USA* **2004**.

[20] T. Mosmann, *J. Immunol. Methods* **1983**, *65*, 55-63.

Table of Contents
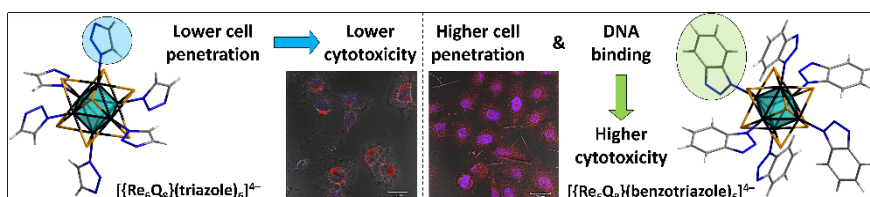
The structure of terminal triazole ligands alter the biological properties of rhenium cluster complexes, in particular their cellular internalization and toxicity profiles. Specifically, unlike clusters with 1,2,3- or 1,2,4-triazole those with benzotriazole ligands demonstrated specific cellular internalization and binding to DNA due to the π-rich benzene unit.